Research Article | Vol. 9, No. 12 | 1 Dec 2018 | BIOMEDICAL OPTICS EXPRESS 6519
Biomedical Optics EXPRESS

Complementary use of polarization-sensitive and standard OCT metrics for enhanced intraoperative differentiation of breast cancer

JIANFENG WANG,[1] YANG XU,[1,2] KELLY J. MESA,[1,2] FREDRICK A. SOUTH,[1,2] ERIC J. CHANEY,[1] DAROLD R. SPILLMAN, JR.,[1] RONIT BARKALIFA,[1] MARINA MARJANOVIC,[1] P. SCOTT CARNEY,[1,2] ANNA M. HIGHAM,[3] Z. GEORGE LIU,[3] AND STEPHEN A. BOPPART[1,2,4,5,*]

[1]*Beckman Institute for Advanced Science and Technology, University of Illinois at Urbana-Champaign, Urbana, Illinois, USA*
[2]*Department of Electrical and Computer Engineering, University of Illinois at Urbana-Champaign, Urbana, Illinois, USA*
[3]*Carle Foundation Hospital, Urbana, Illinois, USA*
[4]*Department of Bioengineering, University of Illinois at Urbana–Champaign, Urbana, Illinois, USA*
[5]*Carle Illinois College of Medicine, University of Illinois at Urbana–Champaign Urbana, Illinois, USA*
**boppart@illinois.edu*

Abstract: We report the development and implementation of an intraoperative polarization-sensitive optical coherence tomography (PS-OCT) system for enhancing breast cancer detection. A total of 3440 PS-OCT images were intraoperatively acquired from 9 human breast specimens diagnosed by H&E histology as healthy fibro-adipose tissue (n = 2), healthy stroma (n = 2), or invasive ductal carcinoma (IDC, n = 5). A standard OCT-based metric (coefficient of variation (CV)) and PS-OCT-based metrics sensitive to biological tissue from birefringence (i.e., retardation and degree of polarization uniformity (DOPU)) were derived from 398 statistically different and independent images selected by correlation coefficient analysis. We found the standard OCT-based metric and PS-OCT-based metrics were complementary for the differentiation of healthy fibro-adipose tissue, healthy stroma, and IDC. While the CV of fibro-adipose tissue was significantly higher (p<0.001) than those of either stroma or IDC, the CV difference between stroma and IDC was minimal. On the other hand, stroma was associated with significantly higher (p<0.001) retardation and significantly lower (p<0.001) DOPU as compared to IDC. By leveraging the complementary information acquired by the intraoperative PS-OCT system, healthy fibro-adipose tissue, healthy stroma, and IDC can be differentiated with an accuracy of 89.4%, demonstrating the potential of PS-OCT as an adjunct modality for enhanced intraoperative differentiation of human breast cancer.

1. Introduction

Breast cancer is the most commonly diagnosed malignancy and the leading cause of cancer death in females worldwide, with an estimated 2.6 million cases and 521,900 deaths occurring in 2012 [1]. Similarly, in the United States, breast cancer has become the most prevalent cancer in females with a total of 266,120 new cases diagnosed and 40,920 deaths reported in 2018 [2]. Current standard-of-care for early-stage and locally advanced breast cancer is breast conserving surgery (BCS) [3], which when followed by radiation therapy, shows improved overall survival and disease-specific survival over mastectomy [4]. During BCS, it is critical to identify and completely resect the tumor and yield negative margins in order to avoid re-excision and improve the quality of life after BCS. Different methods have been developed to assess excised breast tissue specimens in an effort to achieve negative margins. Routine resection of cavity shave margins has been shown to reduce the rates of positive margins, but results in excessive tissue loss which affects postoperative recovery and cosmesis [5]. Additional intraoperative methods including frozen section [6] and touch-prep cytology [7]

346713 https://doi.org/10.1364/BOE.9.006519
Journal © 2018 Received 26 Sep 2018; revised 11 Nov 2018; accepted 12 Nov 2018; published 28 Nov 2018

Biomedical Optics EXPRESS

were also reported. However, these methods are often time-consuming, associated with sampling errors [8] and sample preparation artifacts [9], and are considered impractical for BCS. Therefore, it is imperative to develop intraoperative methods that enable real-time identification of positive margins during BCS.

Various intraoperative methods have been developed for evaluating tumor margins during BCS, including a handheld probe for performing radiofrequency spectral analysis [10,11], quantitative diffuse reflectance imaging [12,13], confocal mosaicking microscopy [14], point spectroscopy [15,16], and optical coherence tomography (OCT) [17–21], among others. OCT, combining high optical resolution, high-speed, and millimeter scale imaging depth, has shown much promise for intraoperative breast tumor margin assessment. In particular, the development of handheld [22] and needle [23,24] OCT probes coupled with portable OCT systems have significantly advanced the application of OCT during BCS. In general, the imaging contrast of standard OCT relies on the variations of refractive index and the light scattering properties of tissue [25]. Specifically, for breast tissue, breast cancer appears more highly scattering than healthy tissue and disrupts the normal structure of fibro-adipose tissue found in the normal breast, making it possible to differentiate the two. However, it remains more challenging to differentiate between normal stroma and tumor, which both appear highly scattering under standard OCT.

Our group has previously demonstrated bench-top polarization-sensitive OCT (PS-OCT) for detecting and quantifying birefringence arising from the differences in collagen content and organization in breast tissues, and demonstrated the potential of PS-OCT to differentiate between stroma and tumor *ex vivo* [26]. In this work, we report the development of an intraoperative PS-OCT system used in the operation room for enhancing the detection and differentiation of invasive ductal carcinoma (IDC). IDC occurs when cancer previously confined to the ductal system spreads into the surrounding tissue microenvironment, and may metastasize to the lymph nodes and throughout the body. IDC makes up nearly 72- 80% of all breast cancer diagnoses and accurate detection of IDC is critical [27]. A standard OCT-based-metric (i.e., coefficient of variation (CV)) and two PS-OCT-based metrics (i.e., retardation and degree of polarization uniformity (DOPU)) were derived for the detection of IDC. The performances of CV, retardation, and DOPU to differentiate fibro-adipose tissue, stroma, and IDC were quantitatively evaluated. Finally, linear discriminant analysis (LDA) and leave-one-tissue-site-out cross-validation (LOSCV) were implemented on the derived metrics to develop robust diagnostic models for the differentiation of fibro-adipose tissue, stroma, and IDC of the human breast.

2. Materials and methods

2.1. Intraoperative polarization-sensitive optical coherence tomography system

A portable custom-designed polarization-sensitive spectral-domain OCT system was developed to be easily maneuvered by one person into the operating room. Figure 1(a) shows the schematic of the intraoperative PS-OCT system. The system used two customized super-luminescent diodes (SLDs) as the source. The two SLDs were centered at 1236 nm and 1346 nm, each having a bandwidth of 81 nm and 118 nm, respectively, and were combined by a 50/50 fiber coupler covering a spectral range of 1200~1400 nm and achieving an axial resolution of 5 μm. The output from the SLDs was first linearly polarized by an in-line linear polarizer (Thorlabs ILP13010PM-APC), then passed through an optical circulator (AFW Technologies PMP-13-R-C3N-45-22), 45 m of polarization-maintaining (PM) fiber to minimize the effects of ghost images [28], and delivered into a free-space Michelson interferometer through PM fibers. The horizontal linearly-polarized light sent into the Michelson interferometer was split into reference and sample arms by a 50/50 non-polarization beam splitter (Thorlabs, BS015). In the reference arm, the horizontal linearly-polarized light passed through a 22.5-degree positioned quarter-waveplate, reflected by a mirror, and then back through the same quarter waveplate where it was finally 45-degree

Biomedical Optics EXPRESS

linearly-polarized light. In the sample arm, the horizontal linearly-polarized light passed through a 45-degree positioned quarter-waveplate, resulting in circularly polarized light which was scanned by a pair of galvo scanners (Thorlabs, GVS102) and incident onto the sample surface after passing through an objective (Thorlabs, LSM02), achieving a transverse resolution of 8 μm. The incident circularly polarized light was changed into elliptically polarized light by the birefringent specimens (i.e., breast tissue), then passed through the same objective and quarter waveplate, and finally interfering with the 45-degree linearly-polarized light of the reference arm. The interference fringes passing through the optical circulator were split by a PM fiber polarizing beam splitter (AC Photonics PBS-13-P-2-2-1-1) and detected by two spectrometers each using 2048 pixel linescan cameras (Sensors Unlimited GL2048L), resulting in a 76 kHz A-scan rate for the system. There were 2048 A-scans for each B-scan/frame. The power at the sample was 3 mW and the sensitivity of the system was 89 dB. Control software written in Labview enabled real-time acquisition and display of the images based on the standard OCT intensity *I* and the PS-OCT-enabled phase retardation δ, which can be calculated as [29]:

$$I = \left|E_{out,1}\right|^2 + \left|E_{out,2}\right|^2 \tag{1}$$

$$\delta = \mathrm{a\,tan}(\left|E_{out,1}\right| / \left|E_{out,2}\right|) \tag{2}$$

where $E_{out,1}$ and $E_{out,2}$ are the intensities measured by the two spectrometers. The Stokes vectors (I,Q,U,V) of the sample can be further calculated by:

$$I = E_{out,1}E_{out,1}^{\ *} + E_{out,2}E_{out,2}^{\ *} \tag{3.1}$$

$$Q = E_{out,1}E_{out,1}^{\ *} - E_{out,2}E_{out,2}^{\ *} \tag{3.2}$$

$$U = 2\left|E_{out,1}\right| / \left|E_{out,2}\right| \cos(\arg(E_{out,1}E_{out,2}^{\ *})) \tag{3.3}$$

$$V = 2\left|E_{out,1}\right| / \left|E_{out,2}\right| \sin(\arg(E_{out,1}E_{out,2}^{\ *})) \tag{3.4}$$

where "*" denotes the complex conjugate, "arg" represents argument.

The degree of polarization uniformity (DOPU) is defined as [30]:

$$DOPU = \sqrt{\bar{Q}^2 + \bar{U}^2 + \bar{V}^2} \tag{4}$$

where

$$(\bar{Q},\bar{U},\bar{V}) = (\sum_i \frac{Q_i}{I_i}, \sum_i \frac{U_i}{I_i}, \sum_i \frac{V_i}{I_i}) \tag{5}$$

and *i* indicates the *i*-th pixel within a spatial kernel by which the DOPU is defined.

The coefficient of variation (CV) is defined as:

$$\mathrm{CV} = \frac{\sqrt{\frac{\sum_i (I_i - \mu)^2}{N-1}}}{\mu} \tag{6}$$

where

$$\mu = \frac{\sum_i I_i}{N} \tag{7}$$

Biomedical Optics EXPRESS

and *i* indicates the *i*-th pixel within a spatial kernel by which CV is calculated. *N* is the overall pixel number within the spatial kernel. The size of the spatial kernel for DOPU and CV calculations was 5 by 5 pixels (25 by 40 μm^2). Both DOPU and CV were computed on linear data.

2.2. Tissue imaging

A total of 9 human subjects undergoing either breast reduction surgery (healthy controls, no history of cancer) (2 patients), or lumpectomy (4 patients) or mastectomy (3 patients) were recruited for this study. Among the 9 subjects recruited, tissue specimen from 2 subjects were diagnosed as healthy fibro-adipose tissue; tissue specimens from 2 subjects were healthy stroma; and homogeneous-appearing tissue specimens from the remaining 5 subjects were diagnosed with different stages of invasive ductal carcinoma (Stage IA: n = 2; Stage IIA: n = 1, Stage IIB: n = 1, Stage IIIA: n = 1). All subjects preoperatively signed an informed consent permitting the investigative use of the tissue, and this study was approved by the Institutional Review Boards (IRB) of both Carle Foundation Hospital and the University of Illinois at Urbana-Champaign. Immediately after surgical resections, *ex vivo* tissue specimens were imaged by the intraoperative PS-OCT system located in the operating room. Areas imaged with PS-OCT were marked with ink for later histological processing, which served as the gold standard for tissue classification. Following formalin fixation, the tissue was processed using standard procedures for histological evaluation of hematoxylin and eosin-stained tissue sections. The paired galvo scanners allowed for 3D volumetric imaging, but due to the time constraints in the operating room, only a single B-scan or a set of B-scans were intraoperatively acquired from each tissue site. As a result, 3440 PS-OCT images were intraoperatively acquired from 75 sites (fibro-adipose tissue: n = 13, stroma: n = 12, IDC: n = 50).

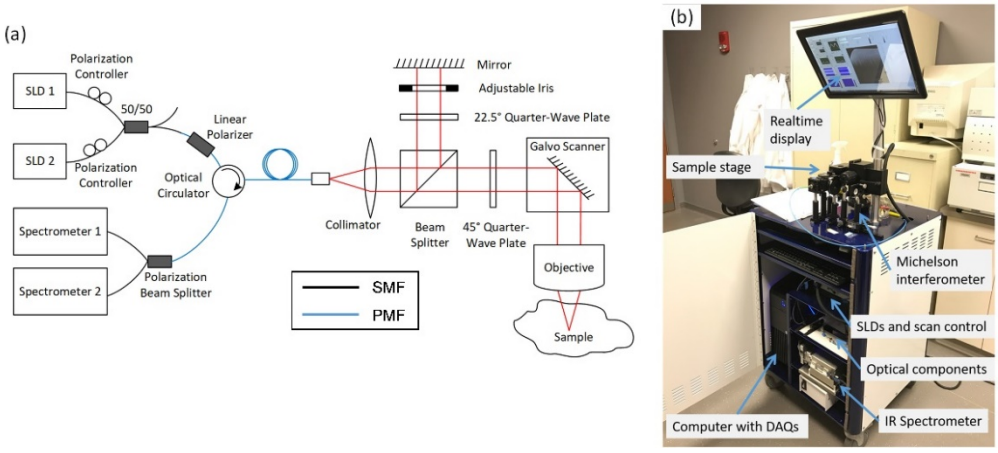

Fig. 1. Intraoperative PS-OCT system. (a) Schematic showing optical hardware components. (b) Intraoperative PS-OCT system integrated in a portable cart for easy transportation into the operating room and positioning near the sterile surgical field. SLD: superluminescent diode; SMF: single mode fiber; PMF: polarization maintaining fiber.

2.3. Statistical analysis

In order to obtain independent analysis and remove classification artifacts arising from images that were closely correlated due to spatial proximity, correlation coefficients were calculated for the images acquired from tissue sites where more than one PS-OCT image was acquired. Correlation coefficient analysis showed that when images were a physical distance of 0.1 mm apart, the correlation coefficients were smaller than 0.01, and the 0.1 mm spatially-separated images were considered as independent. Therefore, from the 9 subjects in this

Biomedical Optics EXPRESS

study, a total of 398 independent images (fibro-adipose tissue: n = 70, stroma: n = 263, IDC: n = 65) from 75 sites (fibro-adipose tissue: n = 13, stroma: n = 12, IDC: n = 50) were finally used for the statistical analysis. A standard OCT-based metric, the coefficient of variance (CV), was chosen for this study because it can compare the intensity variation of image regions that have different intensity means and can be calculated in less than 30 seconds using a standard multi-core desktop PC [31]. PS-OCT-based retardation and DOPU metrics were chosen to reveal the breast tissue form birefringence and could be calculated in less than 1 second using a standard multi-core desktop PC. Further, the means of the CV, retardation, and DOPU were calculated for each image, and the unpaired two-sided Student's *t*-test was used to evaluate their differences among fibro-adipose tissue, stroma, and IDC. Linear discriminant analysis (LDA) was applied on the derived intensity and polarization metrics for developing a diagnosis model. Leave-one-tissue-site-out cross-validation (LOSCV) was further used to assess and optimize the LDA model complexity, while reducing the risk of over-fitting. The above multivariate statistical analysis was performed using in-house written scripts in the Matlab programming environment (Mathworks. Inc., Natick, MA).

3. Results and discussion

As shown in Fig. 2(a), adipocytes are recognizable in the OCT image of fibro-adipose tissue due to their round shape and low scattering lipid interior, while the fibrous septa appear moderately scattering and are identified by their linear vein-like structure. These unique features associated with fibro-adipose tissue demonstrate that standard OCT alone offers the capability to differentiate fibro-adipose tissue from stroma or IDC. Unlike fibro-adipose tissue, however, stroma tissue appears as relatively large areas that are homogeneous and moderately scattering under OCT (Fig. 2(f)), which is similar to IDC (Fig. 2(k)), making it difficult to discriminate IDC from normal stroma under standard OCT alone. The cellular composition of IDC is, however, much different from that of normal stroma. In IDC, tumor cells have displaced the normal breast tissue, resulting in fragmentation and disorganization of the collagen structures leading to lower retardation (Fig. 2(n)) in IDC compared to images of normal stroma. In addition, IDC is associated with higher DOPU (Fig. 2(m)). This is probably because DOPU is a parameter representing the spatial uniformity of polarization, and the randomly-oriented collagen fibers [32] of IDC results in low birefringence and more uniformly distributed polarization states. One notes that thresholding was used to generate masks to only consider image areas with empirically meaningful tissue signal. In Fig. 2, 20% of the CV standard deviation was set as a threshold to generate the mask.

To explore the diagnostic capability of standard OCT- and PS-OCT- based metrics, CV (Figs. 2(b), (g), (l)), DOPU (Figs. 2(c), (h), (m)) and retardation (Figs. 2(d), (i), (n)) were all derived from the PS-OCT measurements. Since fibro-adipose tissue is characterized by relatively uniform honey-comb-like structures and does not appear as homogeneous, a higher CV was expected, as confirmed by the brighter CV image of fibro-adipose tissue (Fig. 2(b)). Further calculation shows the CV of the fibro-adipose tissue is significantly ($p<0.001$) higher than either stroma or IDC (Fig. 3(a)), which is consistent with the CV image (Fig. 2(b)). The CV difference between stroma and IDC, however, is minimal and does not show significant difference. This observation is in agreement with the OCT images of the stroma and IDC, which both appear homogeneous and moderately scattering (Figs. 2(f)(k)). To determine how the CV performs to differentiate between stroma and IDC, a threshold of 5.6 was chosen by optimizing receiver operating characteristic (ROC) curves. With that threshold, fibro-adipose tissue can be differentiated against stroma and IDC with an accuracy of 89.2% (sensitivity: 94.3% (66/70), specificity: 88.1% (289/328)), but the stroma and IDC were all mixed without clear differentiations.

Retardation and DOPU derived from PS-OCT analysis, on the other hand, revealed significant differences between stroma and IDC. For instance, the retardation of stroma was significantly ($p<0.001$) higher than that of IDC, which agrees with the hypothesis that the

Biomedical Optics EXPRESS

tissue birefringence originates from the collagen content. An empirical retardation threshold of 0.82 was chosen by optimizing ROC curves to differentiate stroma from IDC with an accuracy of 86.3% (sensitivity: 87.5% (230/263), specificity: 81.5% (53/65)). Similarly, the DOPU of stroma is significantly (p<0.001) lower than that of IDC. This is because collagen bundles are abundant and well-aligned within stroma, resulting in significant changes in polarization state which lead to lower DOPU values. However, the collagen content of IDC is very sparse, causing little-to-no change in the polarization state which leads to higher DOPU values. An empirical DOPU threshold of 0.78 was chosen by optimizing ROC curves to separate IDC and stroma with an accuracy of 87.8% (sensitivity: 87.5% (230/263), specificity: 89.2% (58/65)). Further inspection of the misclassified PS-OCT images of stroma and IDC revealed brighter ghost images than those that correctly classified PS-OCT images, indicating that the ghost images, even minimized by a long (45 m in this paper) PM fiber, still existed, and lowered the classification accuracy of the PS-OCT-based metrics. We are currently developing next-generation PS-OCT systems without using PM fibers to completely remove these confounding ghost images.

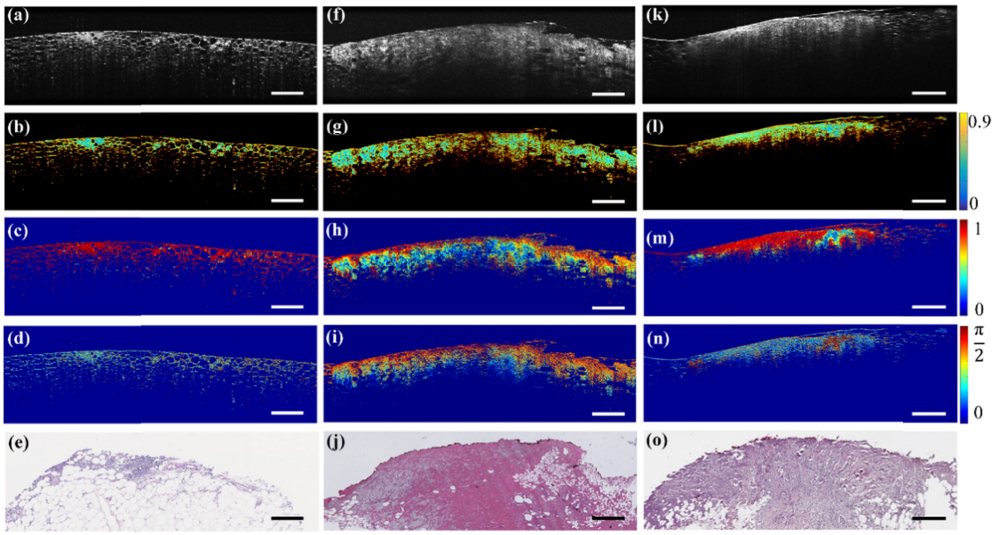

Fig. 2. Representative structural OCT images (a, f, k), coefficient of variation (CV) (b, g, l), degree of polarization uniformity (DOPU) (c, h, m), retardation (d, i, n) and H&E-stained histology (e, j, o) of fibro-adipose tissue (a-e), stroma (f-j), and invasive ductal carcinoma (k-o), respectively. Scale bar: 500 μm. Note, CV (b, g, l) is shown on a base 10 logarithmic scale.

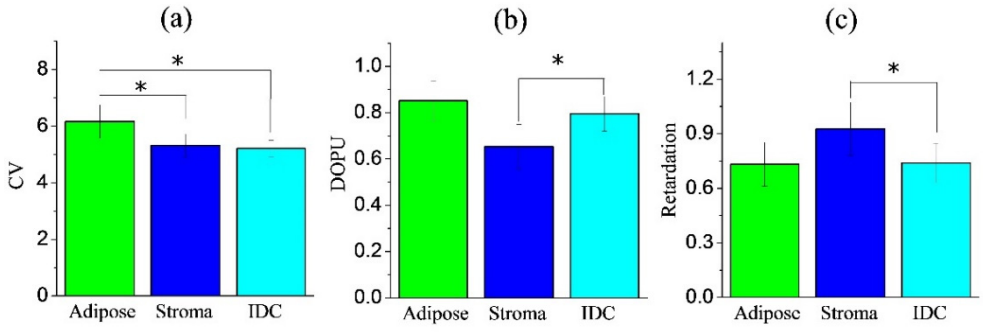

Fig. 3. Bar diagrams ± 1 SD showing the (a) CV, (b) DOPU, and (c) retardation of different tissue types (i.e., adipose, stroma, and IDC) interrogated by the intraoperative PS-OCT system. * p<0.001

Biomedical Optics EXPRESS

As stated above, we found that the OCT intensity-based metric, CV, and the PS-OCT-based metrics, retardation and DOPU, were complementary for the differentiation of IDC. Considered further, the CV exploits the scattering differences between fibro-adipose tissue and that of stroma and IDC, but is not able to distinguish IDC from stroma (Fig. 3(a)). On the other hand, retardation and DOPU indicate collagen fiber distributions and could differentiate stroma and IDC very well (Figs. 3(b-c)). We therefore implemented linear discriminant analysis (LDA) – leave one site out cross-validation (LOSCV) to utilize the complementary information revealed by PS-OCT- and standard OCT-based metrics for the classification of fibro-adipose tissue, stroma, and IDC. With histopathology as the gold standard (prior information), Fig. 4 shows the 2-dimensional ternary plot of the posterior probabilities of each PS-OCT prediction using LDA-LOSCV for PS-OCT measurements. The prediction results are also summarized in Table 1. We found among 70 adipose tissue (column-wise with histopathology as gold standard), 67 were correctly classified into adipose by PS-OCT measurements (row-wise), while the remaining 3 were misclassified as IDC by PS-OCT measurements. Among 263 stroma tissues (column-wise with histopathology as gold standard), 230 were correctly classified into stroma by PS-OCT measurements (row-wise), while 29 were misclassified as adipose and 4 were misclassified as IDC by PS-OCT measurements. Overall, we found fibro-adipose tissue, stroma, and IDC could be detected with an accuracy of 89.2%, confirming the complementary nature of PS-OCT- and standard OCT- based metrics for enhanced differentiation of fibro-adipose, stroma, and IDC.

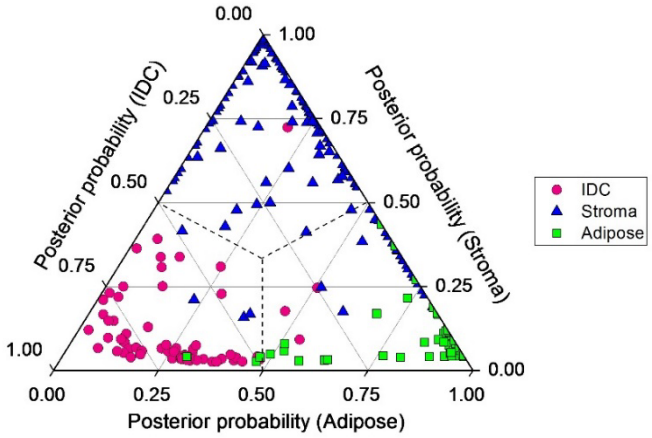

Fig. 4. Posterior probabilities of 398 statistically different PS-OCT measurements belonging to fibro-adipose tissue (n = 70), stroma (n = 263), and IDC (n = 65), based on the PS-OCT and standard OCT techniques.

Table 1. Confusion matrix detailing the multiclass classification results of PS-OCT measurements of different breast tissues using LDA with leave-one tissue site-out, cross-validation methodology.

		Histopathology		
		Adipose	Stroma	IDC
PS-OCT measure-ments	Adipose	67	29	5
	Stroma	0	230	1
	IDC	3	4	59
Sensitivity (%)		95.7	87.5	90.8
Specificity (%)		89.6	80.2	97.9
Accuracy (%)		90.7	91.5	96.7

Biomedical Optics EXPRESS

Some limitations of the current study should be identified. One notes that the number of acquired PS-OCT images are unbalanced, with a relatively larger number of images identified as stroma compared to those identified with breast cancer tissue (e.g., IDC). This is primarily due to the limited number of available specimens, as well as the size and type of specimens that became available. Larger multicenter studies are underway to increase the number of subjects and specimens, and to further assess the clinical detection capabilities of intraoperative PS-OCT for breast tumor margin detection and breast cancer subtyping. Related to specimen availability, only the IDC subtype of breast cancer was investigated in this study. Unlike IDC, ductal carcinoma *in situ* (DCIS) was previously found to be associated with relatively strong birefringence, as demonstrated in our previous work on *ex vivo* differentiation of human breast tissue [26]. A separate study is also currently underway to evaluate the capability of PS-OCT for the differentiation of DCIS.

In addition, the IDC tissues included in the current study were rather homogeneous, with little or no portions of the images being normal. This was intentional so that we could derive numerical metrics (CV, retardation, and DOPU) from each image for statistical analysis. In real margin assessment, we would expect not only homogeneous regions of tissue, but also heterogeneous tissues with a mixture of tumor and normal tissues. To implement the strategy developed in this paper for margin assessment, we would need to segment the images first, and then calculate the means of numerical metrics (CV, retardation, and DOPU) from each segmented area for classification. Alternatively, with windowed-measurements as smaller regions of interest, these numerical metrics could be calculated, compared to the metric values of more homogeneous tissue images (such as in this paper), and then determine a probability of each tissue type for each region of interest. The periodic nature of the cumulative retardation signal used in the current study may also lead to classification inaccuracies, especially when considering the classification of smaller regions of interest. Classification by using local tissue retardation should be explored further.

Finally, this study was performed using an intraoperative PS-OCT system configured with a microscope sample arm. Ongoing work is focused on the miniaturization and integration of the current free-space Michelson interferometer (Fig. 1) into a handheld probe that can be integrated with the current PS-OCT system and utilized by a surgeon for *in vivo* imaging of the tumor resection bed.

4. Conclusions

We have developed and demonstrated an intraoperative PS-OCT system along with an image classification approach for enhanced differentiation of human invasive ductal carcinoma (IDC). Significantly increased coefficients of variation (CV) were observed for fibro-adipose tissue compared to either normal healthy stroma or IDC. While the CV differences between stroma and IDC were minor, significantly increased degree of polarization uniformity (DOPU) and significantly reduced retardation were associated with IDC compared to stroma. By using the complementary information provided by CV, DOPU, and retardation revealed by the PS-OCT/OCT system, an overall accuracy of 89.4% was achieved to differentiate fibro-adipose tissue, stroma, and IDC. This work demonstrates the potential of using PS-OCT as a complementary adjunct imaging modality to OCT for enhanced breast cancer detection in the operation room.

Funding

National Institutes of Health (R01 CA213149 and R01 EB023232).

Acknowledgments

The authors thank the research and surgical nursing staff at Carle Foundation Hospital, Urbana, IL, for their assistance with this study, as well as the subjects who participated in this

Biomedical Optics EXPRESS

research. We also thank Thorlabs, Inc., for their contributions and technical discussions related to this PS-OCT system. Additional information can be found at: http://biophotonics.illinois.edu.

Disclosures

Stephen Boppart is cofounder and chief medical officer of Diagnostic Photonics, Inc., Chicago, Illinois, which is developing and commercializing interferometric synthetic aperture microscopy for applications in intraoperative tumor margin detection. He also receives royalties for patents licensed by the Massachusetts Institute of Technology related to OCT. Other authors have no potential conflicts of interest to disclose.

References

1. L. A. Torre, F. Bray, R. L. Siegel, J. Ferlay, J. Lortet-Tieulent, and A. Jemal, "Global cancer statistics, 2012," CA Cancer J. Clin. **65**(2), 87–108 (2015).
2. American Cancer Society, "Breast Cancer Facts & Figures," (2017–2018).
3. S. E. Singletary, "Surgical margins in patients with early-stage breast cancer treated with breast conservation therapy," Am. J. Surg. **184**(5), 383–393 (2002).
4. E. S. Hwang, D. Y. Lichtensztajn, S. L. Gomez, B. Fowble, and C. A. Clarke, "Survival after lumpectomy and mastectomy for early stage invasive breast cancer: the effect of age and hormone receptor status," Cancer **119**(7), 1402–1411 (2013).
5. A. B. Chagpar, B. K. Killelea, T. N. Tsangaris, M. Butler, K. Stavris, F. Li, X. Yao, V. Bossuyt, M. Harigopal, D. R. Lannin, L. Pusztai, and N. R. Horowitz, "A randomized, controlled trial of cavity shave margins in breast cancer," N. Engl. J. Med. **373**(6), 503–510 (2015).
6. J. M. Jorns, D. Visscher, M. Sabel, T. Breslin, P. Healy, S. Daignaut, J. L. Myers, and A. J. Wu, "Intraoperative frozen section analysis of margins in breast conserving surgery significantly decreases reoperative rates: one-year experience at an ambulatory surgical center," Am. J. Clin. Pathol. **138**(5), 657–669 (2012).
7. F. D'Halluin, P. Tas, S. Rouquette, C. Bendavid, F. Foucher, H. Meshba, J. Blanchot, O. Coué, and J. Levêque, "Intra-operative touch preparation cytology following lumpectomy for breast cancer: a series of 400 procedures," Breast **18**(4), 248–253 (2009).
8. E. L. Rosenthal, J. M. Warram, K. I. Bland, and K. R. Zinn, "The status of contemporary image-guided modalities in oncologic surgery," Ann. Surg. **261**(1), 46–55 (2015).
9. E. K. Valdes, S. K. Boolbol, I. Ali, S. M. Feldman, and J.-M. Cohen, "Intraoperative touch preparation cytology for margin assessment in breast-conservation surgery: does it work for lobular carcinoma?" Ann. Surg. Oncol. **14**(10), 2940–2945 (2007).
10. F. Schnabel, S. K. Boolbol, M. Gittleman, T. Karni, L. Tafra, S. Feldman, A. Police, N. B. Friedman, S. Karlan, D. Holmes, S. C. Willey, M. Carmon, K. Fernandez, S. Akbari, J. Harness, L. Guerra, T. Frazier, K. Lane, R. M. Simmons, A. Estabrook, and T. Allweis, "A randomized prospective study of lumpectomy margin assessment with use of MarginProbe in patients with nonpalpable breast malignancies," Ann. Surg. Oncol. **21**(5), 1589–1595 (2014).
11. M. Thill, "MarginProbe: intraoperative margin assessment during breast conserving surgery by using radiofrequency spectroscopy," Expert Rev. Med. Devices **10**(3), 301–315 (2013).
12. J. Q. Brown, T. M. Bydlon, S. A. Kennedy, M. L. Caldwell, J. E. Gallagher, M. Junker, L. G. Wilke, W. T. Barry, J. Geradts, and N. Ramanujam, "Optical spectral surveillance of breast tissue landscapes for detection of residual disease in breast tumor margins," PLoS One **8**(7), e69906 (2013).
13. B. J. Tromberg, A. Cerussi, N. Shah, M. Compton, A. Durkin, D. Hsiang, J. Butler, and R. Mehta, "Imaging in breast cancer: diffuse optics in breast cancer: detecting tumors in pre-menopausal women and monitoring neoadjuvant chemotherapy," Breast Cancer Res. **7**(6), 279–285 (2005).
14. S. Abeytunge, Y. Li, B. Larson, G. Peterson, E. Seltzer, R. Toledo-Crow, and M. Rajadhyaksha, "Confocal microscopy with strip mosaicing for rapid imaging over large areas of excised tissue," J. Biomed. Opt. **18**(6), 061227 (2013).
15. M. D. Keller, E. Vargis, N. de Matos Granja, R. H. Wilson, M. A. Mycek, M. C. Kelley, and A. Mahadevan-Jansen, "Development of a spatially offset Raman spectroscopy probe for breast tumor surgical margin evaluation," J. Biomed. Opt. **16**(7), 077006 (2011).
16. G. M. Palmer, C. Zhu, T. M. Breslin, F. Xu, K. W. Gilchrist, and N. Ramanujam, "Comparison of multiexcitation fluorescence and diffuse reflectance spectroscopy for the diagnosis of breast cancer (March 2003)," IEEE Trans. Biomed. Eng. **50**(11), 1233–1242 (2003).
17. S. A. Boppart, W. Luo, D. L. Marks, and K. W. Singletary, "Optical coherence tomography: feasibility for basic research and image-guided surgery of breast cancer," Breast Cancer Res. Treat. **84**(2), 85–97 (2004).
18. F. T. Nguyen, A. M. Zysk, E. J. Chaney, J. G. Kotynek, U. J. Oliphant, F. J. Bellafiore, K. M. Rowland, P. A. Johnson, and S. A. Boppart, "Intraoperative evaluation of breast tumor margins with optical coherence tomography," Cancer Res. **69**(22), 8790–8796 (2009).

Biomedical Optics EXPRESS

19. A. M. Zysk, K. Chen, E. Gabrielson, L. Tafra, E. A. May Gonzalez, J. K. Canner, E. B. Schneider, A. J. Cittadine, P. Scott Carney, S. A. Boppart, K. Tsuchiya, K. Sawyer, and L. K. Jacobs, "Intraoperative assessment of final margins with a handheld optical imaging probe during breast-conserving surgery may reduce the reoperation rate: Results of a multicenter study," Ann. Surg. Oncol. **22**(10), 3356–3362 (2015).
20. A. M. Zysk and S. A. Boppart, "Computational methods for analysis of human breast tumor tissue in optical coherence tomography images," J. Biomed. Opt. **11**(5), 054015 (2006).
21. M. Villiger, D. Lorenser, R. A. McLaughlin, B. C. Quirk, R. W. Kirk, B. E. Bouma, and D. D. Sampson, "Deep tissue volume imaging of birefringence through fibre-optic needle probes for the delineation of breast tumour," Sci. Rep. **6**(1), 28771 (2016).
22. S. J. Erickson-Bhatt, R. M. Nolan, N. D. Shemonski, S. G. Adie, J. Putney, D. Darga, D. T. McCormick, A. J. Cittadine, A. M. Zysk, M. Marjanovic, E. J. Chaney, G. L. Monroy, F. A. South, K. A. Cradock, Z. G. Liu, M. Sundaram, P. S. Ray, and S. A. Boppart, "Real-time imaging of the resection bed using a handheld probe to reduce incidence of microscopic positive margins in cancer surgery," Cancer Res. **75**(18), 3706–3712 (2015).
23. R. A. McLaughlin, B. C. Quirk, A. Curatolo, R. W. Kirk, L. Scolaro, D. Lorenser, P. D. Robbins, B. A. Wood, C. M. Saunders, and D. D. Sampson, "Imaging of breast cancer with optical coherence tomography needle probes: feasibility and initial results," IEEE J. Sel. Top. Quantum Electron. **18**(3), 1184–1191 (2012).
24. A. M. Zysk, F. T. Nguyen, E. J. Chaney, J. G. Kotynek, U. J. Oliphant, F. J. Bellafiore, P. A. Johnson, K. M. Rowland, and S. A. Boppart, "Clinical feasibility of microscopically-guided breast needle biopsy using a fiber-optic probe with computer-aided detection," Technol. Cancer Res. Treat. **8**(5), 315–321 (2009).
25. J. Wang, Y. Xu, and S. A. Boppart, "Review of optical coherence tomography in oncology," J. Biomed. Opt. **22**(12), 1–23 (2017).
26. F. A. South, E. J. Chaney, M. Marjanovic, S. G. Adie, and S. A. Boppart, "Differentiation of *ex vivo* human breast tissue using polarization-sensitive optical coherence tomography," Biomed. Opt. Express **5**(10), 3417–3426 (2014).
27. D. P. Arps, P. Healy, L. Zhao, C. G. Kleer, and J. C. Pang, "Invasive ductal carcinoma with lobular features: a comparison study to invasive ductal and invasive lobular carcinomas of the breast," Breast Cancer Res. Treat. **138**(3), 719–726 (2013).
28. M. K. Al-Qaisi and T. Akkin, "Swept-source polarization-sensitive optical coherence tomography based on polarization-maintaining fiber," Opt. Express **18**(4), 3392–3403 (2010).
29. J. F. de Boer, T. E. Milner, M. J. van Gemert, and J. S. Nelson, "Two-dimensional birefringence imaging in biological tissue by polarization-sensitive optical coherence tomography," Opt. Lett. **22**(12), 934–936 (1997).
30. M. J. Ju, Y.-J. Hong, S. Makita, Y. Lim, K. Kurokawa, L. Duan, M. Miura, S. Tang, and Y. Yasuno, "Advanced multi-contrast Jones matrix optical coherence tomography for Doppler and polarization sensitive imaging," Opt. Express **21**(16), 19412–19436 (2013).
31. K. J. Mesa, L. E. Selmic, P. Pande, G. L. Monroy, J. Reagan, J. Samuelson, E. Driskell, J. Li, M. Marjanovic, E. J. Chaney, and S. A. Boppart, "Intraoperative optical coherence tomography for soft tissue sarcoma differentiation and margin identification," Lasers Surg. Med. **49**(3), 240–248 (2017).
32. C. Luparello, "Minireview: Aspects of collagen changes in breast cancer," J. Carcinog. Mutagen. **13**, 7 (2013).